Eur. Phys. J. A (2022) 58:114
https://doi.org/10.1140/epja/s10050-022-00771-1

THE EUROPEAN PHYSICAL JOURNAL A

Review

# Nucleosynthesis in multinucleon transfer reactions

**S. Heinz**[1,2,a], **H. M. Devaraja**[2]

[1] GSI Helmholtzzentrum für Schwerionenforschung GmbH, 64291 Darmstadt, Germany
[2] Justus-Liebig-Universität Giessen, 35392 Giessen, Germany

Received: 21 April 2022 / Accepted: 16 June 2022

Communicated by Nicolas Alamanos

**Abstract** How does one populate still vacant areas on the chart of nuclides? Mainly on the neutron-rich side several thousand further isotopes are expected to exist, including most of the nuclei along the astrophysical r-process path. The standard nucleosynthesis reactions, which are fragmentation, fission and fusion, are reaching their limits. Therefore, other pathways to exotic nuclei are needed. Years ago, the idea arose to revive multinucleon transfer reactions to progress toward the neutron-rich side of heavy and superheavy nuclei. Meanwhile, this option is investigated in nuclear physics labs worldwide. Beside new studies of transfer product kinematics and cross-sections, the development of suitable separation and detection techniques for heavy transfer products is ongoing. But how promising are these new advances? So far achieved results allow us to get an impression on the potential which multinucleon transfer reactions provide for nucleosynthesis.

## Contents



[a] e-mail: s.heinz@gsi.de (corresponding author)

## 1 Introduction

For decades, fragmentation, fission and fusion reactions are versatile tools to produce exotic nuclei in the lab (Fig. 1). Fragmentation is an efficient method to create neutron-deficient as well as neutron-rich isotopes of elements up to the uranium region, while fission is often used to produce intermediate heavy neutron-rich nuclei. To synthesize transuranium and superheavy nuclei, fusion is to date the common method. But the bending of the stability line toward the neutron axis results only in neutron-deficient fusion products. A review on the discovery of nuclides, related reactions and techniques can be found in [1,2].

The capabilities of fusion, fragmentation and fission determine the present limits of the nuclide chart. The smallest accessible cross-sections are currently on the 1 pb level for each of the three reactions. This results in average yields of one nucleus per day in fragmentation reactions and one nucleus per weak in fusion, given by available beam intensities and applicable target thicknesses for the respective reaction. One possibility to extend the nuclide chart is the increase of beam intensities. New powerful facilities are arising in many places to provide 10–100 times higher beam currents, aiming to reach sub-picobarn cross-sections. Examples are the SuperFRS project at the new Facility for Antiproton and Ion Research FAIR at GSI (Germany) [3,4], the SPIRAL2 project at GANIL (France) [5], the HIE-ISOLDE facility at

Published online: 30 June 2022

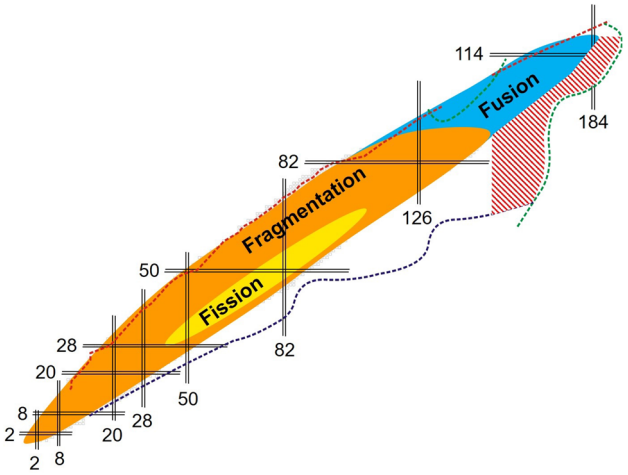


**Fig. 1** Fusion, fragmentation and fission are presently the standard reactions to produce (new) isotopes in the lab. The chart shows the typical areas that are populated with these reactions. The blank area inside the neutron drip-line can principally be populated in fragmentation reactions, but the respective nuclides have not yet been discovered. The red-white hatched area is not accessible with any of the standard reactions

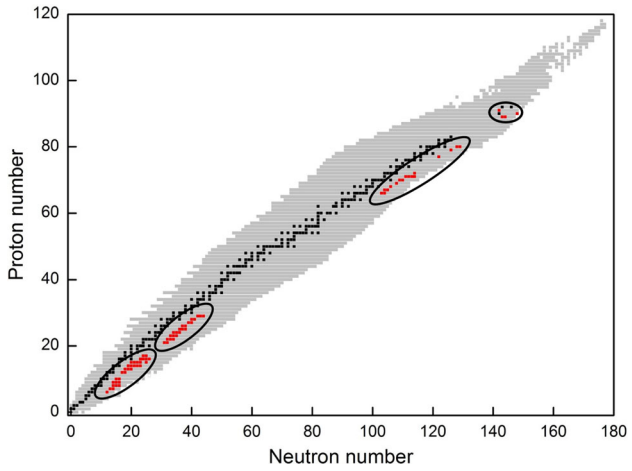


**Fig. 2** Chart of nuclides with the presently known isotopes. The 76 nuclides which were discovered in early MNT experiments during the years 1970–1995 are marked in red. All of them are located on the neutron-rich side

CERN [6], the Radioactive Isotope Beam Factory RIBF at RIKEN Nishina Centre (Japan) [7], or the Facility for Rare Isotope Beams (FRIB) at Michigan State University in the US [8]. Also, a new "superheavy element factory" that is using fusion reactions with intense primary beams is just commencing operations at the Joint Institute for Nuclear Research (JINR) in Dubna, Russia [9].

However, the increase of beam intensities alone will not help to overcome the above described natural restrictions of fragmentation, fission and fusion reactions, which prevent mainly the advance into territory of heavy neutron-rich nuclei. The application of neutron-rich radioactive ion beams (RIBs) would help, but intensities of suitable projectiles are still by many orders of magnitude too small for seriously considering their application on near and mid-term time scales [10–12].

The most promising solution is the reaction type of multi-nucleon transfer (MNT). It occurs in deep inelastic collisions and can be regarded as an incomplete fusion process. First observed in the late 1960s at JINR, MNT reactions immediately revealed their potential for nucleosynthesis. In the years 1970–1995, 76 new isotopes of elements from carbon to thorium were discovered in MNT reactions at JINR, Orsay, Berkeley and GSI [13–27]. All of them are located on the neutron-rich side of the nuclide chart (Fig. 2). Also the capability of MNT reactions to synthesize new superheavy nuclei was investigated. In collisions of projectile beams up to uranium with actinide targets, transfer products up to lawrencium (Z = 103) were observed [28–34]. Among them, $^{260}_{101}$Md was the only *new* isotope discovered then in reactions of $^{18}$O + $^{254}$Es [33].

In the mid-1990s, the investigation of MNT reactions abated. Ten years later it was resumed, given by the necessity to uncover new territory on the nuclide chart and encouraged by promising new model calculations of MNT cross-sections (see e.g. [35–54]) and by new experimental results (see e.g. [10,11,55–71]).

Which advantages offer MNT reactions with respect to complete fusion? Different to fusion, MNT occurs also in very heavy collision systems with total proton and neutron numbers far beyond the ones of heaviest known nuclei. Projectile/target combinations like Xe + Pb (Z = 136) or U + Cm (Z = 188) do principally allow to advance deep into neutron-rich territory, even in the uppermost corner of the nuclide chart. Finally, it is the magnitude of MNT cross-sections and the sensitivity of experimental techniques which will set the limits to their application for nucleosynthesis.

The study of MNT reactions aiming to synthesize new exotic nuclei has become a topical subject in low-energy nuclear physics. It is strongly motivated by understanding the astrophysical r-process path which proceeds through very neutron-rich territory, starting from iron up to uranium, and probably far beyond. In the region of neutron-rich superheavy nuclei new spherical shell closures are predicted at N = 184 and Z = 114, 120 or 126 [72–76], resulting in an enhanced stability of the respective isotopes against fission. This "island of stability" might terminate the r-process. Beside, MNT reactions can also be used to synthesize neutron-rich nuclei below uranium where they compete with fragmentation reactions.

This article will give an overview on the state-of-the-art in nucleosynthesis with MNT reactions and discuss their potential for advancing into still empty areas on the chart of nuclides.

## 2 Multinucleon transfer reactions

### 2.1 Model concept

Multinucleon transfer occurs in deep inelastic binary reactions at energies close to the Coulomb barrier [78–81]. According to the present model concept, the first step to MNT is the formation of a molecule-like dinuclear system (DNS) after capture of projectile and target nucleus due to the nuclear force [78,82]. After capture, the DNS is trapped in a minimum of the nucleus-nucleus potential, followed by a strong exchange of mass (charge) and energy between the reaction partners. Trapping times (i.e. DNS livetimes) are typically on the order of $(10^{-21}$–$10^{-20})$ s and depend on several parameters like proton number, mass (charge) asymmetry, excitation energy or angular momentum of the DNS. During its evolution, the DNS can follow two different pathways which are illustrated in Fig. 3.

If the DNS overcomes the fusion barrier, it evolves into a compound nucleus (CN) and reaches complete statistical equilibrium. The CN de-excites by emitting nucleons and/or gamma rays, or by fission (fusion-fission, FF). Alternatively, the DNS can decay before CN formation (quasi-fission, QF). Before decay, the nuclei can exchange large numbers of neutrons and protons which leads to reaction products far from the original projectile and target nuclei. The excitation energy of the DNS is distributed among the projectile-like and target-like MNT product during the DNS lifetime. After scission of the DNS, the excited primary transfer products (PTP) are emitted. They de-excite by emitting nucleons and $\gamma$ rays. The residual MNT products in their ground state are called secondary transfer products (STP). Alternatively, the excited PTPs can undergo fission for which the probability increases with increasing mass, spin and excitation energy of the nuclei. Such, complete fusion and MNT reactions are closely related processes which both begin with DNS formation.

There are different theoretical models to describe MNT reactions. They are roughly divided into macroscopic, macroscopic-microscopic and purely microscopic models, where the macroscopic-microscopic models are presently the most wide-spread ones. They can again be divided in two main branches. One is the class of DNS models, which use diabatic internuclear potentials, the diffusion master equation and the quantum nature of the interacting nuclei [35–37,40,42–44,83]. Models of the other class use Langevin-type equations of motion and almost adiabatic internuclear potentials [49–52].

The common ground of both approaches is the formation of a DNS and its trapping in the minimum of the nucleus-nucleus potential as first step of the reaction. The reaction dynamics is described by two main degrees of freedom: (i) the relative motion of the interacting nuclei and (ii) the mass and charge transfer between the nuclei. Additional degrees of freedom are the deformation and orientation of the nuclei, the neck degree of freedom, or internal excitations.

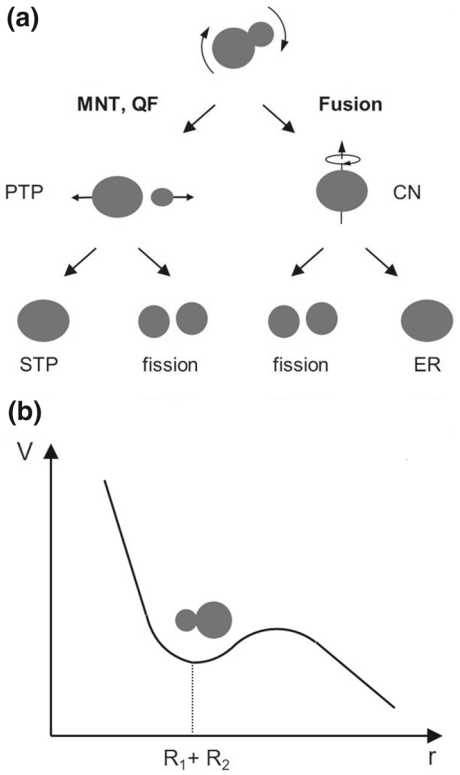


**Fig. 3** **a** The two possible evolution pathways of di-nuclear systems (DNS): once it is formed, the DNS can undergo complete fusion, resulting in a compound nucleus (CN). The de-excitation of the CN proceeds either by evaporating nucleons and $\gamma$ rays, leaving an evaporation residue (ER). Alternatively, the CN can fission. Also, the DNS can scission before reaching the CN state. This process is called quasi-fission (QF). Before QF, large amounts of nucleons can be exchanged between the reaction partners [multinucleon transfer (MNT)]. When the DNS breaks up, the still excited projectile-like and target-like primary transfer products (PTP) are emitted. Their de-excitation takes place by evaporation of nucleons and $\gamma$ rays resulting in the secondary transfer products (STP) or, particularly in the case of heavy nuclei, by fission. **b** Qualitative shape of the nucleus-nucleus potential during a nuclear collision as a function of the distance between the nuclei. $R_1$ and $R_2$ are the radii of the nuclei. The shape of the potential and the depth of the minimum are determined by the interplay between the attractive nuclear force, the repulsive Coulomb force and the angular momentum

The theoretical study of the DNS dynamics allows to consider within a unique approach MNT and fusion reactions. In the DNS model, the nuclear system evolves mainly in the charge (mass) asymmetry coordinate while the internuclear distance R hardly changes. In the Langevin model, the evolution takes place in charge (mass) asymmetry as well as in the R coordinate with evolution of a strong neck between the reaction partners. Both models describe MNT and fusion processes fairly well and show some common trends concerning reaction product cross-sections and kinematics.

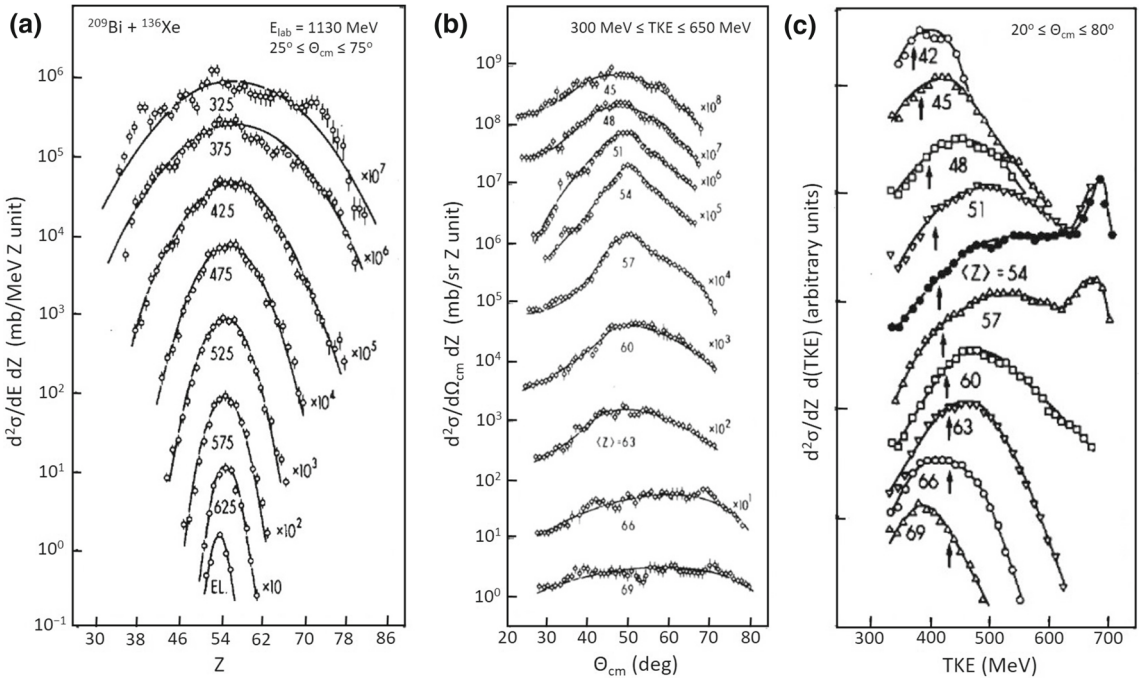


**Fig. 4** Distributions of proton number Z, center-of-mass angle $\theta_{cm}$ and total kinetic energy TKE of binary reaction products from collisions of $^{136}$Xe projectiles with $^{209}$Bi targets at 1130 MeV lab energy. The data were measured at the Lawrence Berkeley Laboratory (LBL) in 1978 [77]. **a** Z distributions of binary reaction products as a function of TKE; respective TKE values are denoted at each curve. **b** Angular distributions of reaction products as a function of their proton number Z; the respective Z is denoted at each curve. **c** TKE distributions of the reaction products as a function of Z; the arrows indicate expected TKE values if a spherical shape of projectile-like and target-like fragment is assumed at the scission point

## 2.2 Kinematics of MNT reactions

The typical features of MNT reaction products are their large variances of mass, charge, energy and angular distributions. It is illustrated in Fig. 4 for transfer products from reactions of $^{136}$Xe + $^{209}$Bi at $E_{lab}$ = 1130 MeV measured in one of the early experiments [77]. The data revealed MNT products which differ by up to 25 protons from the entrance channel nuclei. Also the deep inelastic nature of MNT reactions is revealed in Fig. 4 by the small total kinetic energy (TKE) of the exit channel nuclei.

The large variances of mass, energy and angular distributions indicate also a significant time delay during the reaction, which leads to strong deviations of the MNT product trajectories with respect to the trajectories of elastic and quasi-elastic scattering. Depending on its lifetime, the DNS can perform a full rotation or more before it scissions, which leads to the wide angular distributions of MNT products, resembling the ones of fission fragments [82,84–86]

During the DNS lifetime, kinetic energy is transformed into internal excitation of the DNS. In the utmost case, complete energy dissipation takes place, comparable to compound nucleus reactions. As an example, Fig. 5 shows the TKE of binary reaction products from $^{64}$Ni + $^{208}$Pb collisions measured at the velocity filter SHIP at GSI. Data were taken at six different beam energies ranging from 3% below the interaction barrier to 20% above the barrier [61]. The target-like transfer products were detected at zero degree and originate from central collisions. The TKE values in Fig. 5 are independent of the beam energy which means that the kinematic properties of the exit channel nuclei do no longer depend on the entrance channel properties. Moreover, the TKE values are located at or even below the Viola energy [87]. Normally, the Viola energy is the TKE of fission fragments from an equilibrated CN. TKE values smaller than the Viola energy indicate that the DNS was strongly deformed before scission.

The majority of dissipated energy is transformed into internal excitation of the DNS. By trend, it is shared among the projectile-like and target-like MNT product according to their mass numbers. To observe heavy neutron-rich MNT products it is important to keep excitation energies of the primary transfer products small, to avoid evaporation of large numbers of neutrons. Small excitation energies reduce also the probability for fission of the primary nuclei, which is of particular importance in the actinide and transactinide region where fission barriers are low. In Ni + Pb collisions at SHIP excitation functions of target-like MNT products were measured and revealed a large transfer of nucleons already at

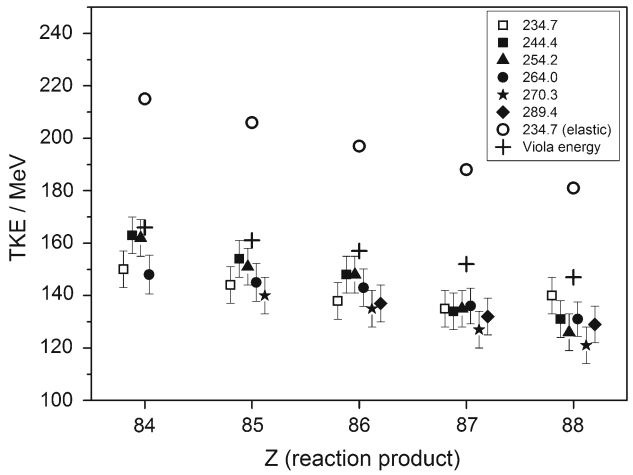


**Fig. 5** Measured total kinetic energy (TKE) as a function of the proton number Z of MNT products created in reactions of $^{64}$Ni + $^{207}$Pb (Z = 110) at beam energies of 4.80, 5.00, 5.20, 5.40, 5.53 and 5.92 MeV/nucleon [61]. The MNT products were detected in forward direction. The beam energies in the center-of-mass frame are given in the inset. The data points for a fixed Z but for different beam energies are plotted with an offset for better discrimination. The energies expected for asymmetric fission fragments of the respective compound nucleus $^{271}$Ds according to the Viola systematics are represented by crosses. The open circles denote the TKE values expected from elastic kinematics at the lowest beam energy

the Coulomb barrier [61]. Respective excitation energies of target-like transfer products were typically few tens of MeV, where on average three neutrons were evaporated.

If one of the emerging MNT products is a magic or near-magic nucleus, shell effects play an important role during the re-distribution of excitation energy among the reaction partners (see e.g. Refs. [61,66,89–91]). Transfer products with closed proton and neutron shells adopt only small excitation energies and the majority of excitation goes to the reaction partner.

### 2.3 Striking similarities

MNT reactions are observed in very different collision systems, from rather light to very heavy ones up to U + U or U + Cm. But despite their diversity, they reveal striking similarities, which were presented and discussed in [54,88]. Figure 6, taken from [88] shows the time evolution of the nuclear systems Ni + Pb (Z = 110) [61], Xe + Pb (Z = 136) [88] and U + U (Z = 184) [60,92]. The evolution of energy dissipation, interaction time and DNS deformation is drawn as a function of the net number of transferred nucleons dA. To enable a direct comparison of the three systems, dA is normalized to the mass number $A_{CN}$ of the respective compound system.

Energy dissipation, interaction time as well as deformation increase quite steeply in the beginning of the reaction and approach saturation after net transfer of about 5% of the total

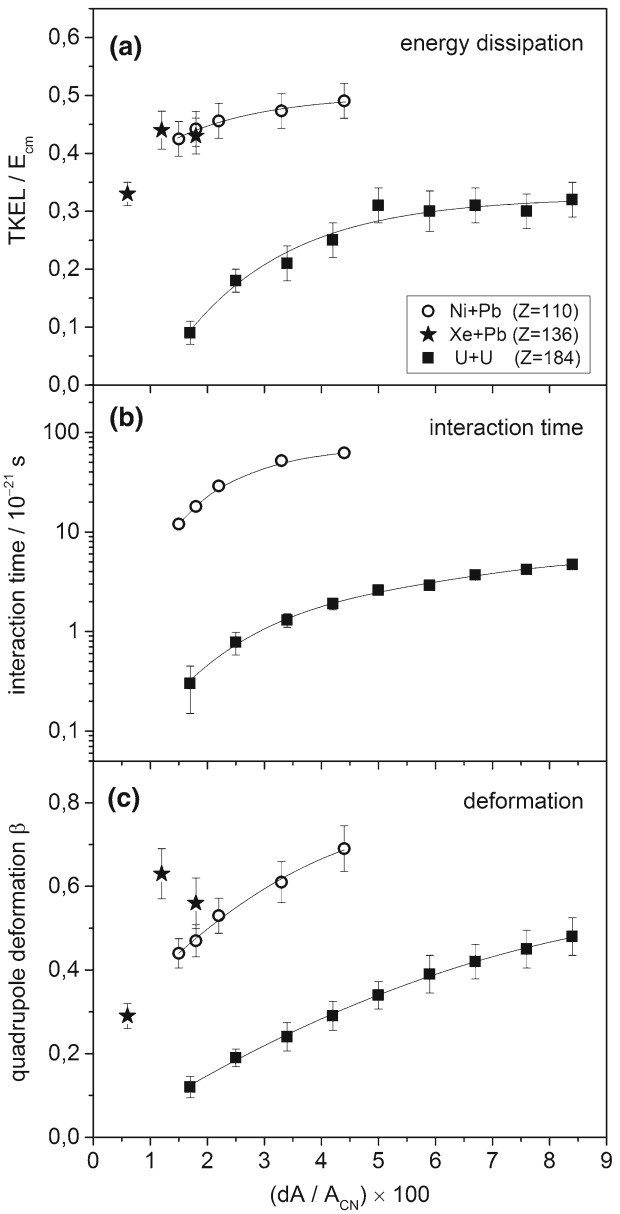


**Fig. 6** Measured total kinetic energy loss TKEL (**a**), interaction times (**b**) and deformations of the exit channel nuclei at the scission point (**c**) for collisions of Ni + Pb ($E_{cm}$ = 289 MeV), Xe + Pb ($E_{cm}$ = 492 MeV) and U + U ($E_{cm}$ = 875 MeV) [88]. On the x-axis scale dA/A is given in percent

nucleon number. This can be interpreted as two phases of the reaction process. Toward small values of $dA/A_{CN}$ the energy dissipation, interaction time and deformation decrease fastly, reflecting that the region of quasi-elastic reactions is entered. The relatively steep slope at the beginning of the curves reveals that in the first stage of the reaction a large amount of energy is dissipated while only a small number of nucleons is transferred (dA $<$ 0.05 $A_{CN}$). Later, the situation reverses and large amounts of nucleons can flow without noticeable increase of energy loss.

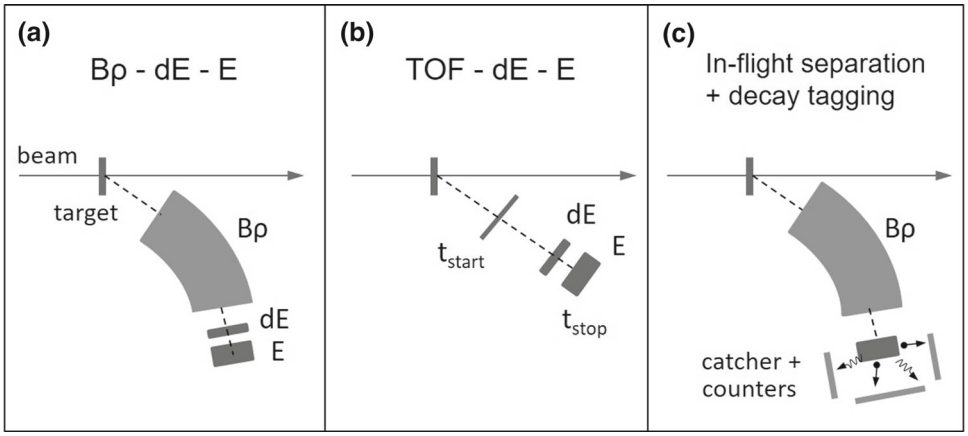


**Fig. 7** Sketch of possible techniques for MNT product identification. **a**, **b** By measuring the kinetic energy E, energy loss dE and time-of-flight (TOF), the mass number A and proton number Z of the reaction products is obtained. The method is suitable for nuclei with mass numbers up to A ≈ 200. It can be combined with separation before the detection system (**a**), or used without separation (**b**). For heavier MNT products, the pulse height deficit becomes relevant. They are to date identified by $\alpha$, $\beta$ and $\gamma$ decay tagging. Usually, in-flight separation with a magnetic separators or a velocity filter is applied before decay tagging (**c**)

Comparing with Fig. 6a one can see that the phase of strong energy dissipation is correlated with a large investment of time. During this phase occurs only a small net transfer of nucleons. Afterwards, when the deep inelastic phase is entered, large numbers of nucleons flow with small friction and time consumption. In this regard the two lighter systems and the heaviest system show very similar characteristics. A difference occurs, however, in the TKE values with respect to the Viola energy. While in Ni + Pb and Xe + Pb TKE reaches values at and even below the Viola energy, in U + U TKE is (10–30)% larger than the Viola energy. However, one must take into account that the extrapolation of the Viola energy to the very distant compound system U +U might be questionable. Also, the absolute values for interaction times are about ten times shorter in U + U. The data indicate that DNS formation still occurs in systems as heavy as Xe + Pb (Z = 136). In the heaviest systems like U + U the strong Coulomb repulsion most probably prevents DNS formation and trapping, but there are clear signatures for the occurrence of deep inelastic reactions and transfer of large numbers of nucleons. The data reveal also that the properties of long-living DNS resemble strongly the ones of compound nuclear systems.

## 3 Experimental techniques in MNT reactions

### 3.1 Measurement of E, dE, TOF

The standard technique to identify A and Z of reaction products is the measurement of their kinetic energy E, kinetic energy loss dE and time-of-flight (TOF). This method was used in early MNT experiments at JINR Dubna, LBL and Orsay. Two different variants of the technique are illustrated in Fig. 7a, b. With the setup of JINR Dubna (Fig. 7a) the MNT products were first separated according to their magnetic rigidity B$\rho$ with a magnetic analyzer. In the focal plane of the analyzer, an E-dE silicon detector telescope was used to determine Z [14,93]. With this method, nearly 30 new projectile-like transfer products of elements from carbon (Z = 6) to chlorine (Z = 17) were observed in reactions of O, Ne and Ar beams with $^{232}$Th targets. The LBL and Orsay groups used TOF-E-dE telescopes like in Fig. 7b [20]. The measurement of TOF allows additionally to determine the mass number A. With this method, a further series of new isotopes of elements from Ca to Zn (Z = 20 to Z = 30) was discovered in MNT reactions of Ar and Fe beams on $^{238}$U targets. The sensitivity limit of the experiments was on the cross-section scale of 1 $\mu$b.

The A and Z resolution obtained with the E-dE-TOF technique is limited by the pulse height deficit, which is strongest for heavy reaction products with low energy. The best mass resolutions which are presently reported are on the order $\Delta$A/A $\approx$ 0.005, which is suitable to identify nuclei up to the region A $\approx$ 200 [94–96].

### 3.2 In-flight separation and decay tagging

Isotope identification of slow and heavy reaction products in the mass region A $\gtrsim$ 200 is to date only possible via their decay properties. In particular $\alpha$ decay tagging is very sensitive. A single decay chain is principally sufficient to pin down the isotope. To reduce background events, separation techniques are usually applied before decay tagging. The

method was already used in early experiments at the GSI Online Mass Separator [25] to identify heavy neutron-rich $\beta$ emitters created in MNT reactions of relatively heavy and symmetric collision systems like Xe + Ta or W + W. After creation, the reaction products were separated according to B$\rho$, then stopped and accumulated in a catcher foil inside an ion source. From there, they were extracted as singly charged ions, re-accelerated to 60 keV and then implanted in a foil again. Using these samples with implanted reaction products, the nuclei were identified offline by $\beta$-, $\gamma$-, and X-ray spectroscopy. With this setup the then heaviest MNT products $^{205}$Au [27] and $^{232,234}$Ac [26] were discovered in collisions of $^{208}$Pb and $^{238}$U beams with W and Ta targets. The sensitivity of the method was on the level of 1 μb.

In more recent experiments, in-flight separation of heavy MNT products at zero degree is performed, where the decay tagging takes place in the focal plane of the separator. Respective experiments are performed at GSI using the velocity filter SHIP [63,64] and the gas-filled separator TASCA [97]. The detection systems consist of an array of position sensitive silicon detectors. In addition, gamma rays are recorded with germanium clover detectors which enables the identification of $\beta$ emitters. Velocity filters and gas-filled separators have already proven their separation capabilities for (super)heavy fusion-evaporation residues since long time. Meanwhile, they demonstrated also their suitability for MNT products. At the velocity filter SHIP the so far heaviest new MNT products, located in the transuranium region, were observed [63,65]. Also, it was the so far most sensitive MNT experiments with cross-section limits of 0.5 nb, reached in a few hours of beamtime.

The fast in-flight separation allows one to detect short-living nuclei with half-lives down to microseconds. But due to the narrow acceptance angles of in-flight separators, only forward emitted MNT products reach the detection system. Typical angular efficiencies are a few permille to few percent, depending on collision system and beam energy.

### 3.3 Radiochemical techniques

Some of the early MNT experiments which started in the 1970s used radiochemical techniques to separate and identify heavy MNT products. Respective experiments were performed at LBL, JINR Dubna and GSI by a collaboration of nuclear chemists [29–32,34,77]. One can distinguish the online and the offline technique. With the offline method, the reaction products were implanted in a thick target or in a catcher foil. Chemical separation was applied to produce samples containing isotopes of the same element. Then, the $\alpha$ decays of each sample were recorded for isotope identification. The minimum time for a full separation and measurement cycle was about 30 minutes, which determines the minimum accessible half-lives of the nuclei.

For shorter-living nuclides, the online technique was used. The nuclei were produced in a helium gas filled target chamber and transported by gas-jet technique to chemical separation devices to separate the different chemical elements. After separation, samples were prepared for identification of the isotopes by decay tagging. The minimum time for one such cycle was about 60 s. The radiochemical methods were very sensitive resulting in lower limit cross-sections of 20 nb. They were mainly applied for MNT products in the actinide region.

The radiochemical methods allow to collect MNT products in their full range of emission angles. However, the technique is relatively slow and restricted to nuclei with half-lives of minutes or longer.

### 3.4 Laser resonance ionisation

Another possibility of heavy isotope identification is the selective laser resonance ionization of the MNT products. A dedicated facility named KEK Isotope Separation System (KISS) was setup at the Radioactive Ion Beam Factory at RIKEN in Japan. It aims mainly for the investigation of neutron-rich MNT products below Pb [69,70,99]. A sketch of the KISS setup is shown in Fig. 8. First, the created MNT products are stopped in an argon gas filled ion catcher which is doughnut-shaped to prevent the primary beam from entering the ion catcher. Laser ionization inside the catcher is used for Z selection. After extraction from the gas cell, the reaction products are passing a magnetic dipole field for A/q separation. The selected ions can then be guided to a detection system for spectroscopic studies or precision mass measurements. At KISS, the mass measurements are performed with a high-resolution multi-reflection time-of-flight mass spectrometer [98].

The laser ionisation method is applicable for nuclei with minimum lifetimes of about 1 s. This time is mainly determined by the extraction time from the gas catcher which is about 0.5 s. The overall efficiency of the present KISS setup is on the scale of 0.1%.

### 3.5 Precision mass measurements

Reaction products can be identified if their mass is measured with sufficiently high resolution to distinguish different isobars. For that one needs mass resolving powers of $m/\Delta m = (10^5 - 10^6)$. Multiple reflection time-of-flight mass spectrometers (MR-TOF-MS) are appropriate devices to reach these resolutions. In MNT reactions a broad region of isotopes is populated which results usually in the appearance of several isobars for each A, containing also already known ones. Therefore, the mass parabola will comprise also known masses beside the new ones and the location of the new mass on the parabola will identify the nucleus, even if

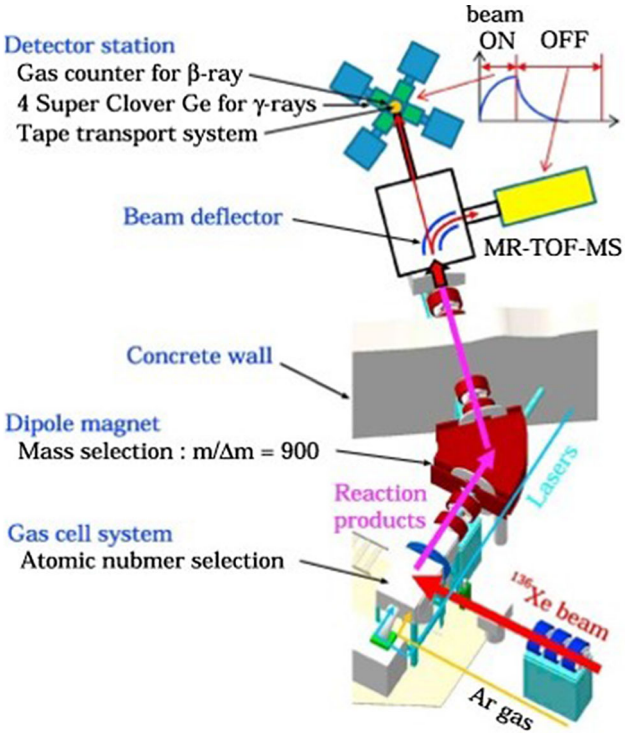


**Fig. 8** Sketch of the KEK Isotope Separation System (KISS) at RIKEN in Japan for laser resonance ionization of reaction products [98]. After stopping in an ion catcher, the Z of MNT or other reaction products is determined by selective laser ionization. A magnetic dipole field after the ion catcher allows for A/q separation. After separation, spectroscopic studies or precision mass measurements can be performed

Z is not directly determined. Investigations of such a method are ongoing at the GSI fragment separator (FRS) facility and at the IGISOL facility at university of Jyväskylä, Finland [100–102]. The setups use a cryogenic stopping cell and an MR-TOF-MS.

The idea is to install targets with thicknesses of several 10 μm inside the stopping cell which is filled with helium gas to stop the reaction products. This allows one to collect reaction products emitted to a wide angular range, which is particularly important for MNT products. The relativistic beams from FRS are decelerated by degraders, such that its mean energy is about 10 MeV/nucleon when it impinges the reaction target inside the ion catcher. The stopped reaction products are extracted and injected to the MR-TOF-MS which allows for the broadband detection of various isotopes. For a mass measurement with sufficient resolution, about 10 nuclei are needed. The method allows one to detect nuclei with half-lives of 10 ms or longer. In order to avoid space charge effects in the stopping cell, the maximum beam intensity is limited. Estimates for uranium beams arrived at maximum intensities of $10^7$ ions per pulse. According to simulations, the method requires presently reaction product cross-sections of minimum 100 μb [103].

### 3.6 Which technique is the best one?

The ideal experimental setup to observe new, heavy exotic MNT products should (i) have a large angular acceptance, (ii) allow to detect MNT products independent of their decay properties and (iii) be sensitive to single nuclei with cross-sections on the picobarn scale and below. Only, we are far from having a technique which fulfills these requirements.

Table 1 summarizes established and new techniques for MNT product identification and their specific features. To date, the radiochemical techniques and the in-flight separation with a velocity filter are the most sensitive methods which allowed to observe heavy MNT products with cross-sections on the 10 and 0.5 nb level, respectively. Important is, that these sensitivities are only reached for $\alpha$ emitters where one or few decay chains are sufficient to pin down the isotope. For $\beta$ emitters, the limit cross-section is about 1000 times higher and amounts to microbarns.

The radiochemical and in-flight techniques are complementary to each other. The radiochemical method allows to collect MNT products in their full angular range, but it is relatively slow and requires isotope lifetimes on the scale of minutes or longer. The in-flight technique is fast and mainly limited by the flight-time of the reaction products through the separator, which is on the scale of 1 μs. But the method has a small angular efficiency and only (0.1–1)% of the reaction products enter the separator. For experiments in near future, the two techniques appear presently as the most promising ones to observe (new) heavy MNT products.

The methods of laser ionization and precision mass measurements are new techniques in this field and still in development. Their motivation is to have a universal method which makes heavy isotope identification independent of the decay

**Table 1** Overview on separation and detection techniques for MNT products. $\sigma_{min}$ is the respective smallest MNT cross-section which was so far measured with the denoted technique and $\tau_{min}$ is the minimum necessary lifetime of a reaction product to be detected with the respective technique

| Experimental technique | $\sigma_{min}$ | $\tau_{min}$ |
|---|---|---|
| E-dE-TOF-B$\rho$ | ~ 1 μb | 0.1–1 μs |
| Velocity filter + $\alpha$ decay tagging | ~ 0.5 nb | ~ 1 μs |
| Velocity filter + $\gamma$ decay tagging | ~ 1 μb | ~ 1 μs |
| Radiochemistry + $\alpha$ decay tagging | ~ 20 nb | ~ 1 min. (online tech.) |
| | | ~ 30 min. (offline tech.) |
| Laser ionization | | ~ 1 s |
| Precision mass measurements | | ~ 1 s |

properties. Both techniques use ion catchers to stop the reaction products before identification. The overall efficiencies are not yet high enough to use them in near future for the production of new (super)heavy MNT products.

## 4 Nucleosynthesis in MNT reactions

### 4.1 Transuranium and superheavy nuclei

#### *4.1.1 State of the art*

In the 1970s and 1980s the radiochemical experiments demonstrated that actinide nuclei up to lawrencium (Z = 103) are populated in MNT reactions. Projectile beams of $^{16,18}$O, $^{20,22}$Ne, $^{40,44,48}$Ca, and $^{238}$U were used in combination with $^{238}$U, $^{248}$Cm and $^{254}$Es targets at energies up to 20% above the Coulomb barrier [28–32,34]. Many of the observed nuclides were located on the neutron-rich side of the stability line. However, no new isotopes were observed and finally fusion reactions made the race for producing nuclei in the transuranium and superheavy element region.

New experimental advances into the transuranium region with MNT reactions started around the year 2010 at the velocity filter SHIP of GSI. In collisions of $^{48}$Ca beams with $^{248}$Cm and $^{238}$U targets more than 100 different MNT products in the region beyond Pb were observed, where the heaviest one was $^{260}_{102}$No [63,64]. For this isotope the to date smallest MNT cross-section of $\sim$0.5 nb was measured [65]. The same experiments revealed also for the first time new transuranium isotopes. All of them are quite neutron-deficient and located around the N = 126 shell. The total of so far known MNT products with proton numbers Z $\geq$ 92 are summarized in Fig. 9.

Theoretical cross-sections and isotope distributions of transuranium and superheavy MNT products are available from DNS and Langevin model calculations [36,104,105]. The different models diverge in their results concerning the optimal projectile-target combinations. The DNS model in [36] suggests to use intermediate heavy neutron-rich projectiles like $^{48}$Ca combined with the heaviest available actinide targets like Pu, Cm or Cf. Collisions of two very heavy nuclei are found to be not suitable in that model because of very short interaction times which do not allow for a massive transfer of nucleons. In comparison, calculations in [104,105] observe MNT products far from the entrance channel nuclei also in collisions of such heavy systems like U + Cm or U + Cf.

Figure 10 shows, as an example, Langevin model calculations of cross-sections for MNT products up to Z = 110 which emerge from collisions of uranium beams with U, Cm and Es targets [104]. Experimental data for U + U [28] and for U + Cm [29] are also shown in Fig. 10. The model calculations reasonably well describe the experimental cross-sections. A maximum deviation of less than an order of magnitude is observed only in a few cases. Theoretical and experimental data reveal a steep decrease of cross-sections by an order of magnitude for every transfer of a proton from projectile to target nucleus. For example, in $^{238}$U + $^{248}$Cm reactions the cross-sections of new neutron-rich Fm isotopes are $\leq$ 50 nb and for new isotopes of No and Sg they reach values of $\leq$ 2 nb and $\leq$ 0.1 pb, respectively.

From the different model predictions no clear trend becomes apparent if giant collision systems, such as U + Cm, or rather systems with intermediate heavy projectiles like Ca+Cm lead to larger cross-sections. For example, DNS model cross-sections [36] for MNT products around Z = 100 are smaller than the respective Langevin model cross-sections [104]. However, the cross-section decrease with increasing MNT product proton number is less steep in the DNS model. Variations are also observed if one compares different model calculations for the same collision system and comparable beam energy. Cross-sections vary within few orders of magnitude for new MNT products in the transuranium region. For example, predicted cross-sections for the

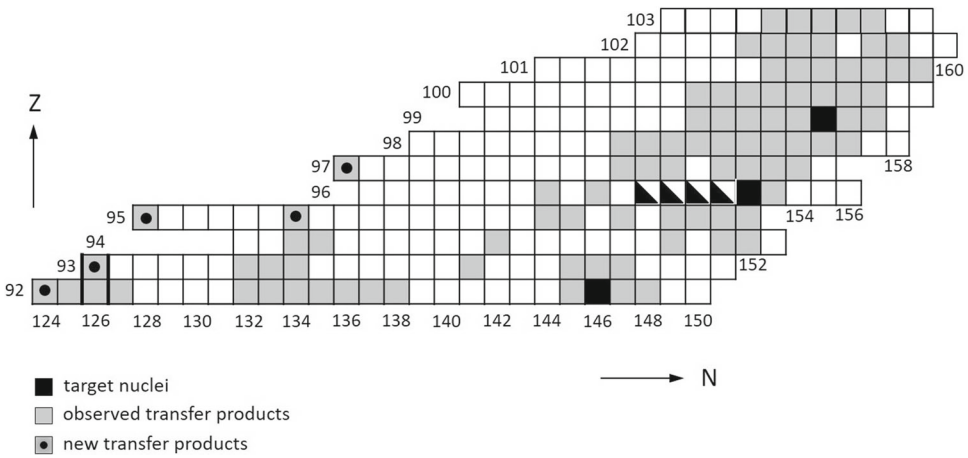


**Fig. 9** Uranium and transuranium isotopes observed in MNT reactions of diverse projectile nuclei with U, Cm, Cf and Es targets. The chart contains the collective of experimental results from radiochemical experiments and from experiments at the velocity filter SHIP. The five new neutron-deficient nuclides which were observed at SHIP are marked by dots

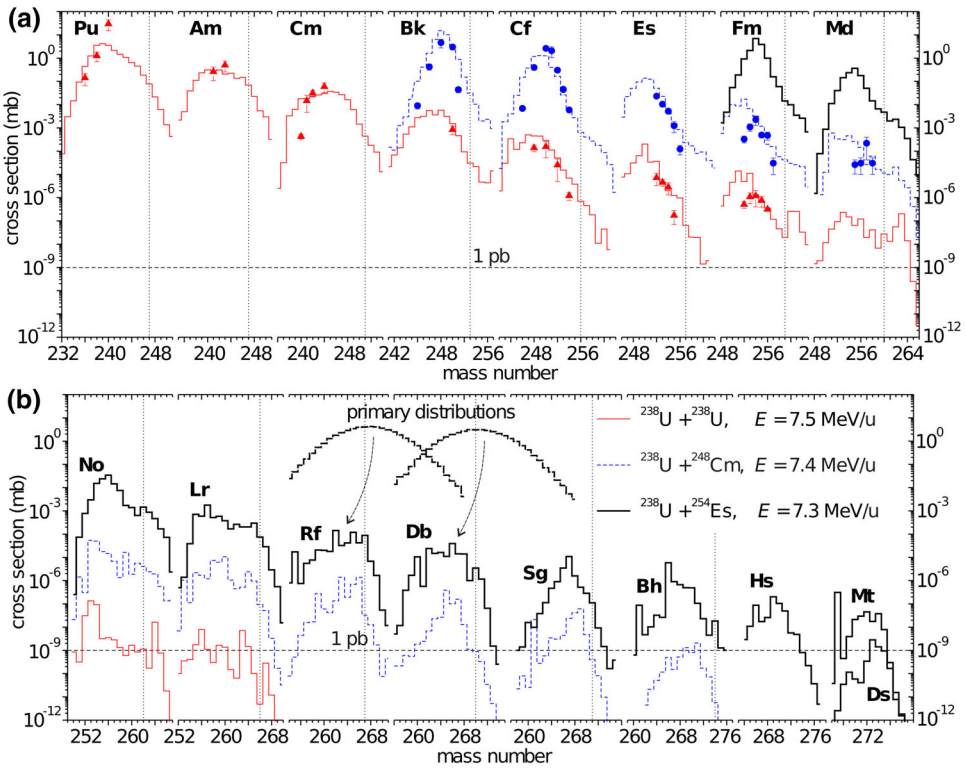


**Fig. 10** Isotopic distributions of the above-target products obtained in collisions of actinides. The thin, dashed, and thick histograms correspond to the results of the calculations [104] for the reactions $^{238}$U + $^{238}$U (E = 7.5 MeV/u), $^{238}$U + $^{248}$Cm (E = 7.4 MeV/u), and $^{238}$U + $^{254}$Es (E = 7.3 MeV/u), respectively. The experimental data for the $^{238}$U + $^{238}$U reaction (triangles) are taken from Ref. [28], and for $^{238}$U + $^{248}$Cm (circles) are from Ref. [29]. For more details, see the text. The heaviest known isotopes of the given chemical elements are indicated by vertical dotted lines. The thick dashed curves show primary (before neutron evaporation) isotopic distributions of Rf and Db in the $^{238}$U + $^{254}$Es reaction

MNT product $^{261}$No are 0.04 nb [36], 0.5 nb [106] (both from collisions of $^{48}$Ca +$^{248}$ Cm) and 5 nb in collisions of $^{238}$U +$^{248}$ Cm [104]. The calculations were performed for energies at the Coulomb barrier.

### *4.1.2 What can we expect?*

How far can we advance with MNT reactions in the region of neutron-rich superheavy nuclei? Figure 11 shows the superheavy element section of the nuclide chart. It comprises about 150 isotopes, synthesized in fusion evaporation reactions or by $\alpha$ decays of mother isotopes. The magenta coloured squares mark still unknown nuclides which can be expected from MNT reactions in future experiments according to Langevin model calculations for $^{238}$U + $^{248}$Cm reactions [104]. Only isotopes with calculated cross-sections of minimum 1 pb are marked in the chart. Accordingly, we can expect about 25 new isotopes of elements Z = (100–106) with neutron numbers N $\leq$ 166. They include most of the not yet directly produced endpoint nuclei of known hot fusion decay chains. The DNS model arrives at very similar results and finds MNT cross-sections between 0.5 nb and 1 pb for neutron-rich isotopes of elements Z = (101–107) in collisions of $^{48}$Ca + $^{248}$Cm [36]. However, nuclei in that region undergo fission or $\beta$ decays and the techniques for their identification are not yet sensitive enough to access (sub)naonobarn cross-sections.

There are another 50 still unknown superheavy isotopes which can be synthesized in the "conventional" way in fusion reactions with stable projectile beams, for example by using Cm or Cf targets. They are marked by an "F" in Fig. 11. These nuclei would fill the gap on the nuclide chart which appears between isotopes produced in cold and in hot fusion reactions. Filling these gaps would link the presently isolated region of relatively neutron-rich superheavy nuclei to the well established part of the nuclide chart.

Remains the region of predicted spherical shell closures at Z = 114, 120 and N = 184. The extrapolation of theoretical cross-sections arrives at values in the sub-femtobarn region for these nuclei, which is far from feasibility, even on a long time scale. However, there might be an "emergency solution" to gain experimental information about the "island of stability". There are superheavy collision systems of neutron-rich radioactive ion beams with heavy targets, which provide a sufficient number of neutrons to reach the N = 184 shell. For complete fusion reactions, the cross-sections and also intensities of radioactive ion beams are by far too small, but quasi-fission and fusion-fission reactions can occur. As discussed in Sect. 2, theoretical and experimental data reveal that the evolution of a DNS toward statistical equilibrium proceeds smoothly and the properties of very long-living DNS resemble already the ones of compound nuclei. The internal properties of the DNS are revealed by the isotope distributions, energy and angular distributions of QF and FF products (see e.g. Refs. [86,107]), and also the influence of shell closures in

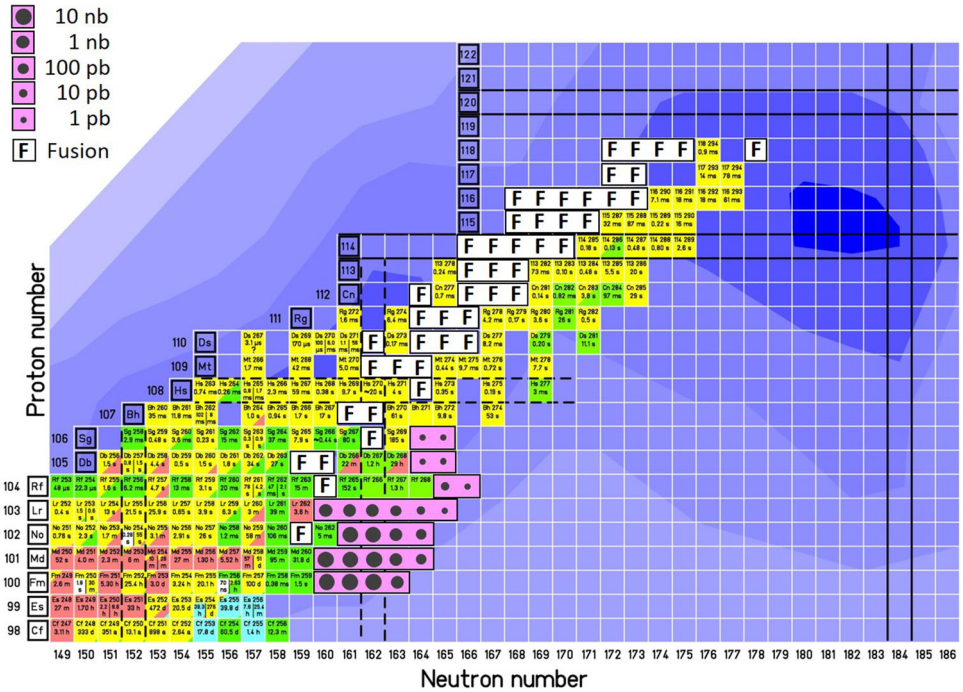


**Fig. 11** Chart of Nuclides with the known isotopes of superheavy elements. The blue background represents shell correction energies (i.e. fission barriers) calculated in the macroscopic-microscopic model [72]. The chart contains three still empty, but very interesting regions: (i) the island of enhanced stability around N = 184, Z = 114 or 120, where spherical shell closures are expected; (ii) the endpoint nuclei of the decay chains of the most neutron-rich known isotopes, which were so far not produced directly and (iii) nuclei which fill the gaps between isotopes produced in hot and cold fusion reactions. The nuclei in area (iii), marked by white squares, can be produced in fusion reactions with stable beams and $^{248}$Cm targets, for example. To produce decay chain endpoint nuclei of area (ii), MNT reactions must be applied. The pink coloured squares indicate the most neutron-rich MNT products which can be obtained with $^{248}$Cm targets and cross-sections of $\geq$ 1 pb. The "island of stability" is far outside the present capabilities of fusion and MNT reactions

the DNS might be revealed by the kinematic properties and isotope distributions of binary reaction products. We have an approved experimental program at CERNs HIE-ISOLDE facility to study QF and FF reactions in collisions of Rb beams with Bi targets [108]. This combination allows for creating DNS with Z = 120, N = 184. Here one has to remark that the choice of collision system is still strongly constrained by the availability of sufficiently intense neutron-rich beams which must be provided with at least $10^6$ ions/s.

### *4.1.3 Unexpected results*

Among the (trans)uranium MNT products in Fig. 9 there are several rather neutron-deficient isotopes [63]. They were observed in $^{48}$Ca + $^{248}$Cm collisions at SHIP at a beam energy slightly above the Coulomb barrier. Among the observed nuclei are also five new isotopes with Z $\geq$ 92. The short halflives and long $\alpha$ decay chains of nuclei in this region allow their relatively easy identification by $\alpha$ decay tagging.

Usually, neutron-deficient nuclei around uranium are synthesized in fusion-evaporation reactions, but a comparison of MNT and fusion yields for these nuclei revealed an interesting result. In Fig. 12 we compare measured fusion residue cross-sections of various uranium isotopes [109–115] with

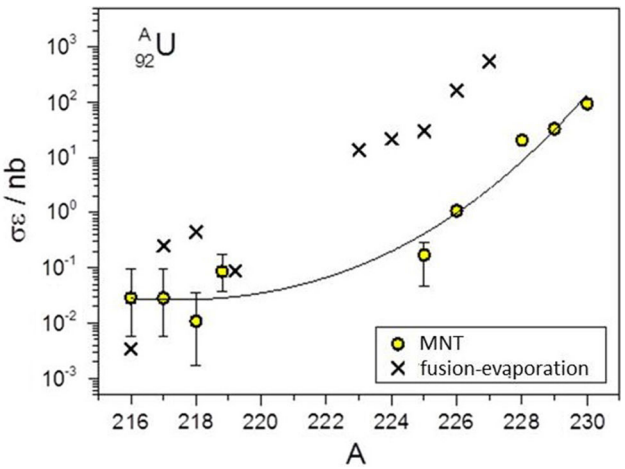


**Fig. 12** The product of cross-section and experimental efficiency, $\sigma\epsilon$, for uranium isotopes measured in fusion-evaporation reactions [109–115] (crosses) and in MNT reactions $^{48}$Ca + $^{248}$Cm [64] (open circles). For $^{219}$U a small offset on the A value is put to avoid an overlap of the data points from complete fusion and MNT

MNT cross-sections measured at SHIP. Figure 12 is a representative example because the behavior is very similar for isotopes of other elements in the uranium region. If fusion cross-sections from more than one experiment were available for the same isotope, we put the largest known value. Instead of the pure production cross-sections, we took the product of cross-section and experimental efficiency, $\sigma\epsilon$, because this is the relevant parameter which reflects the event count rate if one assumes similar beam intensities and target thicknesses. For MNT as well as fusion reactions, $\epsilon$ is mainly determined by the angular acceptance of the applied separators.

It is revealed that the values of $\sigma\epsilon$ for MNT and fusion products tend to approximate each other for very neutron-deficient isotopes close to the N = 126 shell, despite the small angular efficiency of the velocity filter for MNT products. Therefore, in the very neutron-deficient transuranium region, MNT reactions might indeed become an attractive option to synthesize new isotopes. Here one can profit from the broad excitation functions of MNT products which leads to a wide-band population of many different nuclides with sizeable yields in the same experiment, while fusion reactions are only selective on very few specific isotopes.

## 4.2 Neutron-rich r-process nuclei with Z < 82

### *4.2.1 State of the art*

Fragmentation and fission are the standard reactions to produce neutron-rich nuclei below Pb. But model calculations revealed MNT cross-sections which are comparable to, or even larger than fragmentation cross-sections [37,50,52,119]. Figure 13 shows, as an example, Langevin model calculations of MNT cross-sections for isotopes of elements Yb (Z = 70) to Ra (Z = 88) created in reactions of $^{136}$Xe + $^{208}$Pb [50,52]. The Langevin model suggests the application of heavy beams like $^{136}$Xe on Pb or Pt targets, where projectile and target nucleus have similar A/Z.

Cross-section calculations for nuclei along N = 126 were also performed with other models. DNS model calculations in Refs. [37,119] are resulting in cross-sections of similar magnitude, but suggest the application of intermediate heavy neutron-rich beams like $^{48}$Ca or $^{64}$Ni. As discussed earlier, this reflects the stronger dominance of the Coulomb force over the nuclear force in the respective model, making very heavy systems unfavorable. Further, Zhu et al. investigated MNT reactions in various heavy systems like W + U or Xe + Pt by using the model which is based on the DNS approach and the isospin-dependent quantum molecular dynamics model [41,120,121]. The results of different models can vary by several orders of magnitude for the same MNT product like shown in Table 2 exemplary for the isotope $^{204}$Pt.

**Table 2** Predicted cross-sections of $^{204}$Pt isotopes produced in MNT reactions with the denoted collision systems. The results originate from different theoretical models

| Collision system | Cross-section | Refs. |
|---|---|---|
| $^{136}$Xe + $^{208}$Pb | 8 μb | [50] |
| $^{136}$Xe + $^{208}$Pb | 200 μb | [52] |
| $^{48}$Ca + $^{196}$Pt | 20 nb | [119] |
| $^{48}$Ca + $^{238}$U | 0.4 nb | [37] |

In the early years of 2000, Krolas et al. performed MNT experiments in the below-Pb region at Legnaro using reac-

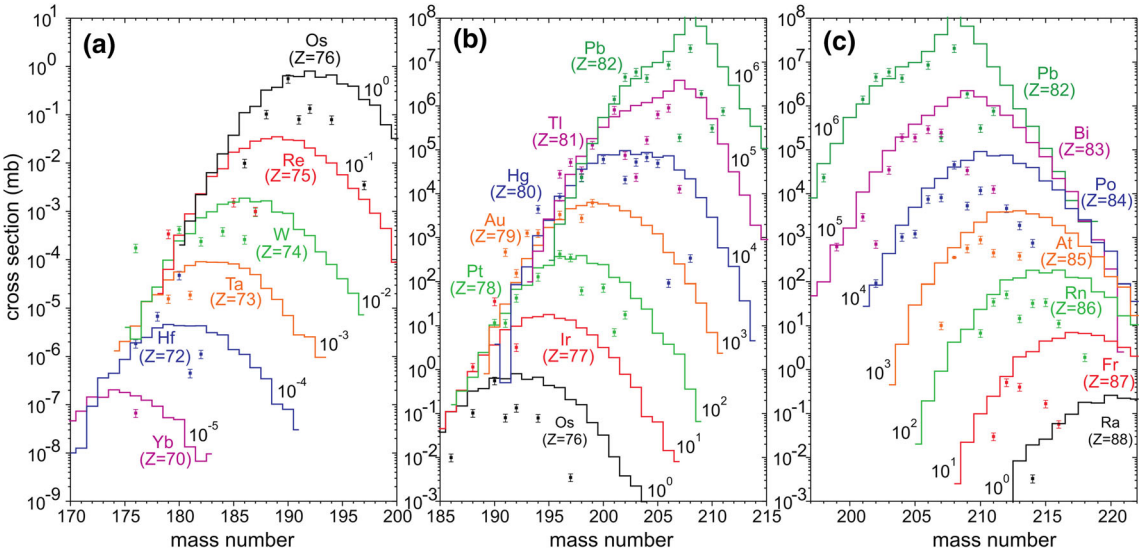


**Fig. 13** Calculated (histograms, Langevin model [52]) and measured [67] (symbols) cross-sections for isotopes of elements Z = (70–88) produced in MNT reactions of $^{136}$Xe+$^{208}$Pb

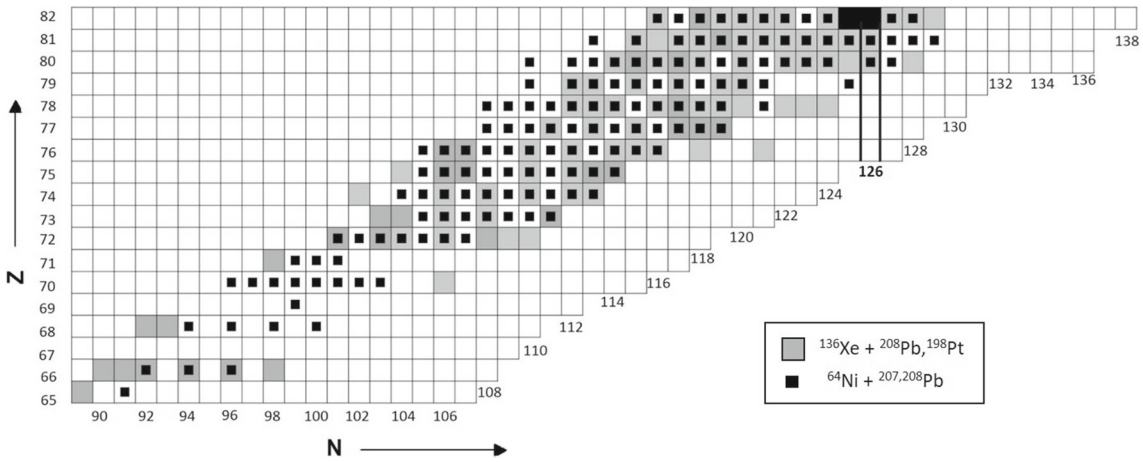


**Fig. 14** Section of the chart of nuclides showing MNT products in the region below Pb which were populated in different experiments. The gray squares represent MNT products observed in reactions of $^{136}$Xe beams with $^{208}$Pb and $^{198}$Pt targets [67,68]. The small black squares indicate MNT products from the reactions $^{64}$Ni +$^{207,208}$Pb [58,62]. The limits of the chart given on the neutron-rich side correspond to the limits of the current Karlsruhe chart of nuclides of 2018

tions of $^{58,64}$Ni + $^{208}$Pb and the thick-target method [58,59]. The reaction products were stopped in the target and yield distributions were established by in-beam and off-line $\gamma$ spectroscopy. A huge number of target-like MNT products of elements from Gd (Z = 64) to Ra (Z = 88) was identified. More recent studies, also using the thick-target technique, were performed at the Argonne National Laboratory (ANL) with reactions of $^{136}$Xe + $^{208}$Pb [67]. Also here, a wide region of projectile-like and target-like MNT products from Z = 48 to Z = 88 was observed in offline $\gamma$ spectroscopy. Beside, experiments were performed at the velocity filter SHIP using reactions of $^{64}$Ni + $^{207}$Pb [62] where MNT products of elements Z = (76–89) were detected. The MNT products were separated at forward angles according to their velocities and identified by $\gamma$ spectroscopy in the focal plane of SHIP. The current sensitivity limit in all these experiments is on the level of (1–10) μb. The chart in Fig. 14 shows all MNT products with $Z \leq 82$ which were observed to date. No new isotopes are among them. The N = 126 shell is only reached for MNT products with $Z \geq 80$. Isotopes from fragmentation and fission reactions still determine the present limits of the nuclide chart on the neutron-rich side.

The MNT cross-sections measured in the individual experiments reveal an astoundingly uniform picture, despite the different experimental techniques and collision systems. Figure 15 shows MNT cross-sections of isotopes with Z = (65–83) measured in reactions of $^{64}$Ni + $^{207}$Pb, $^{136}$Xe + $^{208}$Pb and $^{136}$Xe + $^{196}$Pt by different groups. Cross-sections from fragmentation reactions are also shown. The maximum MNT cross-sections which were reached in the different experiments are very similar and amount to several millibarns for isotopes around the stability valley. The isotopic distributions measured with the heavy and neutron-rich $^{136}$Xe beams are shifted by about five neutrons toward the neutron-rich side with respect to the distributions obtained with $^{64}$Ni beams.

### *4.2.2 What can we expect?*

Experimental data confirm that MNT cross-sections are similar to fragmentation cross-sections and tend to overtake fragmentation toward the neutron-rich side (Fig. 15). It is also revealed experimentally and theoretically that more neutrons in the collision system shift the isotopic distributions of MNT products toward the neutron-rich side. Therefore, heavy, neutron-rich beams like $^{136}$Xe appear more favorable than intermediate heavy beams like $^{64}$Ni. Also, the application of neutron-rich radioactive projectiles leads to neutron-rich MNT products. However, the choice of suitable exotic projectiles with sufficient intensities is quite restricted. Best suitable are isotopes of heavy alkali elements like rubidium or cesium and noble gases like Xe, because they are available with good intensity for a broad region of their exotic isotopes. But still, the intensities of stable, neutron-rich beams like $^{48}$Ca or $^{136}$Xe are several orders of magnitude larger (see also respective discussions in [12]).

An interesting trend was observed by Watanabe et al. in collisions of $^{136}$Xe + $^{198}$Pt [69]. At the GANIL VAMOS spectrometer they measured the isotopic distributions of Xe-like MNT products and deduced from them the ones of target-like nuclei. Watanabe et al. observed that MNT cross-sections overtake fragmentation cross-sections toward decreasing proton number of the MNT products. This trend is also slightly indicated in Fig. 15 by the data of other groups where the target-like isotopic distributions were measured

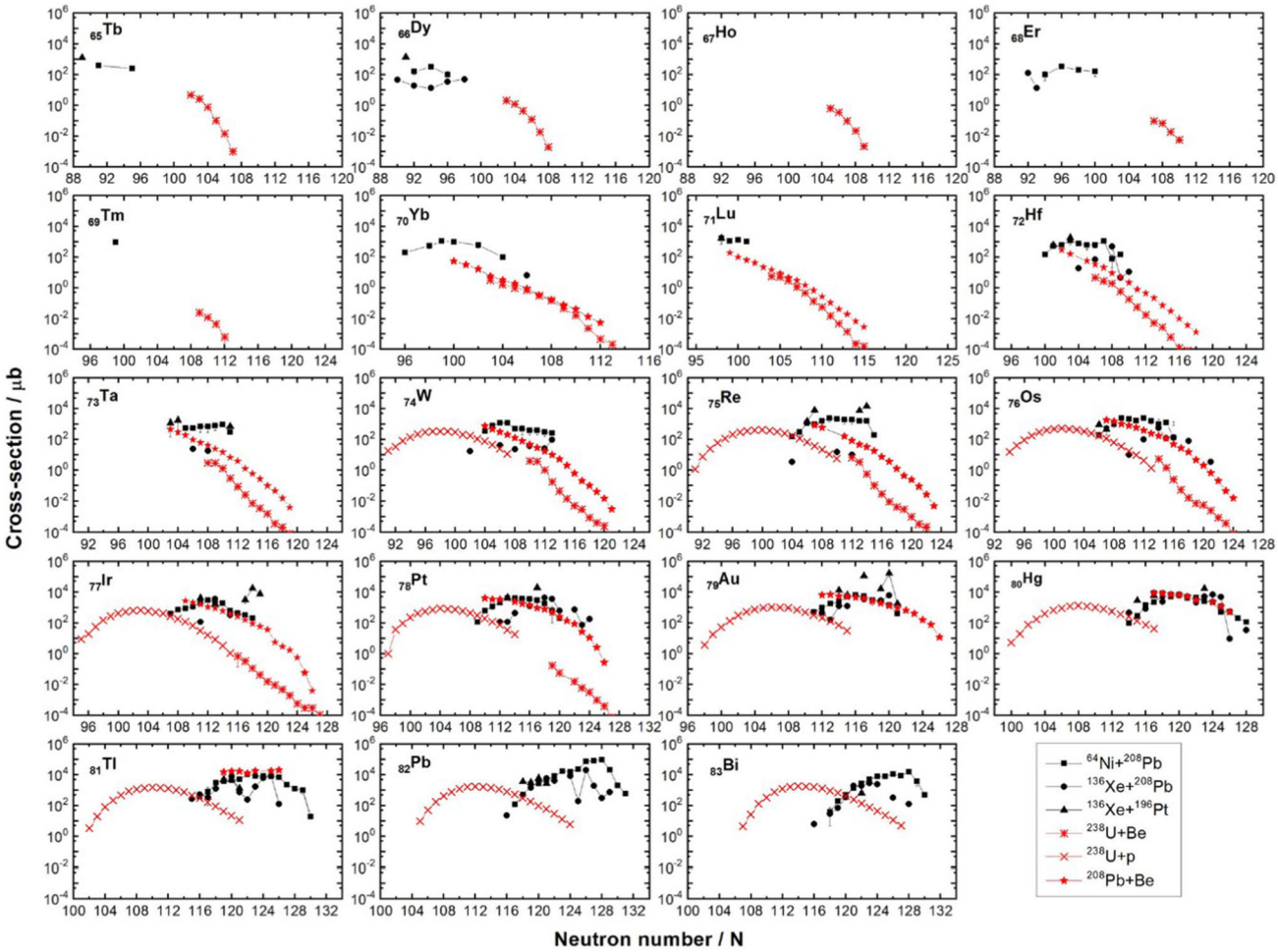


**Fig. 15** Cross-sections of Tb to Bi isotopes produced in MNT reactions. Full squares represent the data from $^{64}$Ni + $^{208}$Pb collisions [58] performed at Legnaro. Full circles denote data from the experiment with $^{136}$Xe + $^{208}$Pb [67] and full triangles represent the data from the experiment $^{136}$Xe + $^{208}$Pt [68] collisions performed at Gammasphere facility of Argonne National Laboratory. The cross-sections measured in fragmentation reactions are shown by asterisks for $^{238}$U+Be [116], crosses for $^{238}$U+p [117], and stars for $^{208}$Pb+Be [118] reactions. In fragmentation reactions, isotopes with still several more neutrons were discovered so far (see Fig. 14 and Ref. [116], but they are not all displayed here

directly. The trend becomes more pronounced toward the neutron-rich side.

Figure 16 shows exemplary the cross-sections for N = 126 isotones from MNT and fragmentation reactions, where the above described trend is well visible. It results from the limited number of available neutrons in fragmentation reactions, which is in the maximum case N = 146 if uranium is applied as beam or target nucleus. In MNT reactions of heavy systems like Xe + Pb more than 200 neutrons participate which causes a flatter decrease of cross-sections toward the neutron-rich side.

### *4.2.3 MNT or fragmentation?*

Apart from production cross-sections there are several further aspects which determine the capability of a reaction type to produce new isotopes. Finally, not only cross-sections but yields are decisive for the experimental feasibility. They include parameters like beam intensity, applicable target thickness and efficiency of the experimental setup. The yield N at the target is the product of cross-section $\sigma$, beam intensity $I_{beam}$ and target thickness $d_T$. The efficiency $\epsilon$ of the detection system and possibly applied separation techniques further reduces the yield. Finally, the measured yield can be expressed as: $N = \sigma \times I_{beam} \times d_T \times \epsilon$.

The parameters which determine the yields are quite different in MNT and fragmentation reactions. Fragmentation reactions at relativistic energies apply targets thicknesses of $10\,g/cm^2$, while in MNT reactions at Coulomb barrier energies target thicknesses are about 1 mg/cm$^2$.

Figure 17 compares the yields of below-Pb isotopes produced in MNT and in fragmentation reactions. The underlying cross-sections were taken from Fig. 15 (parameters for

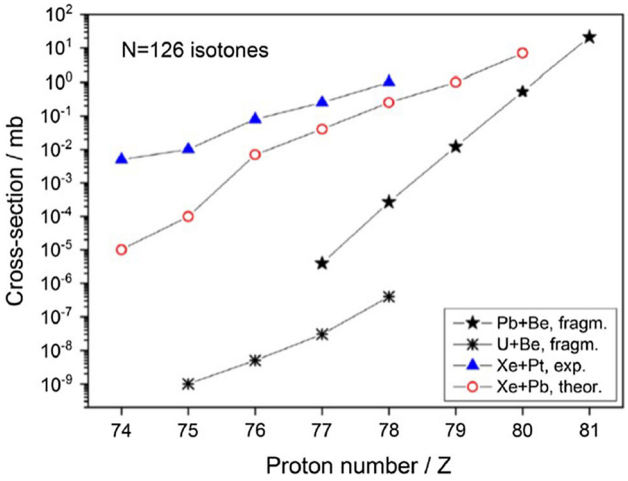


**Fig. 16** Cross-sections of N = 126 isotones with the given Z from transfer and fragmentation reactions. We made this figure according to [69] and added the graphs for U + Be fragmentation reactions [116] and calculated cross-sections for transfer reactions in Xe + Pb [52]

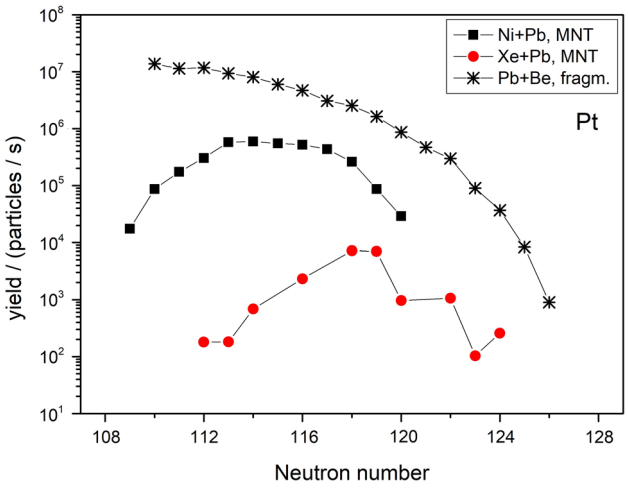


**Fig. 17** Expected count rates per second of Pt isotopes produced in MNT reactions of Ni + Pb and Xe + Pb and in fragmentation reactions. The count rates were calculated from the cross-sections Fig. 15 for Pt isotopes measured in fragmentation reactions of $^{208}$Pb (1 GeV/u)+Be [116] and in transfer reactions of $^{64}$Ni+$^{208}$Pb [58] and $^{136}$Xe+$^{208}$Pb [67]. We assumed the realistic values of beam intensities and target thicknesses denoted in the following. Fragmentation: I(Pb) = $10^{10}$/s, d(Be) = 5 g/cm$^2$; MNT: I(Ni) = $5 \times 10^{12}$/s, d(Pb) = 50 mg/cm$^2$, I(Xe) = $5 \times 10^{10}$/s, d(Pb) = 50 mg/cm$^2$. The count rates are given at the target and do not include possible losses which occur during separation and detection of the nuclei at the individual setups

beam current and target thicknesses are given in the figure caption). Note that the yields in Fig. 15 are given at the target and do therefore not yet include the efficiencies of experimental setups which can vary strongly between individual experiments.

The overall trend indicates that the expected yields seem in favor of fragmentation reactions, mainly given by the possibility to use 10,000 times thicker targets. Apart from this, projectile fragmentation reactions combine further advantages which make them much more efficient than MNT reactions: (i) projectile fragments are emitted to a very narrow forward cone, enabling efficient and fast In-flight separation while MNT products are emitted in a wide angular range which makes their collection/separation ineffective; (ii) A and Z identification of the relativistic fragments can be performed with the $E - \Delta E - TOF - B\rho$ method which makes identification independent of decay properties. Also, the method is very sensitive and is in principle applicable for a single event. In contrast, the lack of sufficiently sensitive identification techniques for $\beta$-decaying MNT products is still a serious bottleneck. The most efficient method is to date $\gamma$ spectroscopy which results in sensitivities on the microbarn level. According to model calculations one can principally observe neutron-rich MNT products up to the boarder of the present chart of nuclides. For the observation of new isotopes, future experiments must be sensitive to sub-microbarn cross-sections.

## 5 Summary

Multinucleon transfer reactions are studied as a pathway to new exotic nuclei, where two still empty areas on the nuclide chart are in the focus of interest. One is the region of neutron-rich superheavy nuclei where also new spherical shell closures are expected at N = 184, Z = 114, 120 or 126. Nuclei in that region cannot be synthesized in fusion reactions with stable projectiles. MNT reactions in very heavy systems like U+Cm would principally be a pathway to produce them. The second region is neutron-rich nuclei below Pb, which are expected to participate in the astrophysical r-process. These nuclei are usually produced in fragmentation or fission reactions. But experimental data and model calculations revealed quite large MNT cross-sections in that region which are comparable to, or even larger than fragmentation cross-sections. By trend, MNT cross-sections increasingly overtake those of fragmentation with increasing neutron number and decreasing proton number of the product nuclei.

The heaviest nuclei which were to date observed in transfer reactions are $^{260}_{102}$No (velocity filter SHIP) and $^{260}_{103}$Lr (radiochemical experiments). For $^{260}_{102}$No also the so far smallest MNT cross-section of 0.5 nb was measured, resulting in the observation of three events in about two hours of irradiation time. With improved experimental setups it appears realistic to reach 1 pb cross-sections in future MNT experiments. Assuming this limit value, we can expect on the neutron-rich side about 25 new isotopes of elements Z = (100–106) and N $\leq$ 166, including the endpoint nuclei of hot fusion decay chains.

About 50 new superheavy isotopes from $Z = (104-118)$ can still be produced in "conventional" fusion reactions

with stable projectiles on actinide targets, which will fill the present gap between the regions of cold and hot fusion-evaporation residues.

Not reachable on a short- or mid-term time scale appear nuclei on and around the predicted "island of stability" at N = 184, Z = 114 or 120–126 for which (sub)femtobarn MNT cross-sections are expected. However, one can expect indirect information about possible enhanced nuclear stability in that area, for example by studying quasi-fission and fusion-fission reactions with neutron-rich radioactive ion beams, which occur with large cross-sections up to the 100 mb scale. Shell closures in the compound nuclear system might leave their fingerprint not only in fusion-evaporation residues but also in the mass, angle and energy distributions of quasi-fission and fusion-fission fragments.

In the neutron-rich area below Pb, the sensitivity limit in MNT reactions is presently on the level of 1 μb, while it is 1 pb in fragmentation reactions. Also, there is a competition of experimental techniques for MNT and fragmentation product separation and identification in that region, which is presently in favour of fragmentation reactions. Future MNT experiments will reveal if the increase of MNT cross-sections toward the neutron-rich side compared to fragmentation can overcompensate the technical advantages of fragmentation reactions.

Finally, experiments at the velocity filter SHIP revealed a large potential for nucleosynthesis with MNT reactions in the very neutron-deficient transuranium region. The first new transuranium MNT products were observed there. Normally, neutron-deficient transuranium nuclei are synthesized in fusion reactions. But the experiments showed that yields from complete fusion and MNT are comparable in that area. However, MNT reactions are more efficient, because a huge number of different isotopes is populated at the same experimental setting due to the broad excitation functions of MNT products, while fusion reactions produce only few isotopes.

**Acknowledgements** Part of this work was supported by DFG grants HE 5469/3-1, HE 5469/3-2 and DE 2946/1-1.

**Funding Information** Open Access funding enabled and organized by Projekt DEAL.

**Data Availability Statement** This manuscript has no associated data or the data will not be deposited. [Authors' comment: Any data that support the findings of this study are included in the article.]



## References

1. M. Thoennessen, Rep. Prog. Phys. **76**, 056301 (2013)
2. M. Thoennessen, *The Discovery of Isotopes, A Complete Compilation* (Springer International Publishing, Cham, 2016)
3. H. Geissel et al., Nucl. Instrum. Methods B **204**, 71 (2003)
4. M. Winkler et al., Nucl. Instrum. Methods B **266**, 4183 (2008)
5. S. Gales, Nucl. Phys. A **834**, 717c (2010)
6. M. Lindroos, P.A. Butler, M. Huyse, K. Riisager, Nucl. Instrum. Methods B **266**, 4687 (2008)
7. J.Y. Yano, Nucl. Instrum. Methods B **261**, 1009 (2007)
8. A. Gade, B.M. Sherrill, Phys. Scr. **91**, 053003 (2016)
9. S. Dmitriev, M. Itkis, Y. Oganessian, EPJ Web Conf. **131**, 08001 (2016)
10. W.D. Loveland, Phys. Rev. C **76**, 014612 (2007)
11. W.D. Loveland, Front. Phys. **7**, 1 (2019)
12. G.G. Adamian, N.V. Antonenko, A. Diaz-Torres, S. Heinz, Eur. Phys. J. A **56**, 47 (2020)
13. J. Wilczynski, V.V. Volkov, P. Decowski, Yad. Fiz. **5**, 942 (1967)
14. A.G. Artukh, G.F. Gridnev, V.L. Mikheev, V.V. Volkov, Nucl. Phys. A **137**, 348 (1969)
15. G.F. Gridnev, V.V. Volkov, J. Wilczynski, Nucl. Phys. A **142**, 385 (1970)
16. A.G. Artukh, V.V. Avdeichikov, G.F. Gridnev et al., Nucl. Phys. A **176**, 284 (1971)
17. A.G. Artukh, G.F. Gridnev, V.L. Mikheev et al., Nucl. Phys. A **211**, 299 (1973)
18. A.G. Artukh, J. Wilczynski, V.V. Volkov et al., Yad. Fiz. **17**, 1126 (1973)
19. A.G. Artukh, G.F. Gridnev, V.L. Mikheev et al., Nucl. Phys. A **215**, 91 (1973)
20. J. Galin, D. Guerreau, M. Lefort et al., Nucl. Phys. A **159**, 461 (1970)
21. F. Hanappe, M. Lefort, C. Ngo et al., Phys. Rev. Lett. **32**, 738 (1974)
22. L.G. Moretto, D. Heunemann, R.C. Jared et al., *Physics and Chemistry of Fission 1973*, vol. 2 (IAEA, Vienna, 1974), p. 351
23. K.L. Wolf, J.P. Unik, J.R. Huizenga et al., Phys. Rev. Lett. **33**, 1105 (1974)
24. S.G. Thompson, L.G. Moretto, R.C. Jared et al., Phys. Scr. Suppl. A **10**, 36 (1974)
25. C. Bruske, K.H. Burkard, W. Huller et al., Nucl. Instrum. Methods Phys. Res. **186**, 61 (1981)
26. K.-L. Gippert et al., Nucl. Phys. A **453**, 1 (1986)
27. Ch. Wennemann, W.-D. Schmidt-Ott, T. Hild et al., Z. Phys. A **347**, 185 (1994)
28. M. Schädel, J.V. Kratz, H. Ahrens et al., Phys. Rev. Lett. **41**, 469 (1978)
29. M. Schädel, W. Brüchle, H. Gäggeler et al., Phys. Rev. Lett. **48**, 852 (1982)
30. H. Gäggeler, W. Brüchle, M. Brügger et al., Phys. Rev. C **33**, 1983 (1986)
31. D. Lee, H. von Gunten, B. Jacak et al., Phys. Rev. C **25**, 286 (1982)
32. D.C. Hoffman et al., Phys. Rev. C **31**, 1763 (1985)
33. E.K. Hulet et al., Phys. Rev. C **40**, 770 (1989)
34. A. Türler et al., Phys. Rev. C **46**, 1364 (1992)
35. G.G. Adamian, N.V. Antonenko, W. Scheid, Phys. Rev. C **68**, 034601 (2003)
36. G.G. Adamian, N.V. Antonenko, A.S. Zubov, Phys. Rev. C **71**, 034603 (2005)

37. G.G. Adamian, N.V. Antonenko, V.V. Sargsyan, W. Scheid, Phys. Rev. C **81**, 057602 (2010)
38. N. Wang, Z. Li, X. Wu, Phys. Rev. C **65**, 064608 (2002)
39. N. Wang, L. Guo, Phys. Lett. B **760**, 236 (2016)
40. Z.-Q. Feng, G.-M. Jin, J.-Q. Li, Phys. Rev. C **80**, 067601 (2009)
41. Z.-Q. Feng, Phys. Rev. C **95**, 024615 (2017)
42. L. Zhu, J. Su, P.-W. Wen, Phys. Rev. C **95**, 044608 (2017)
43. L. Zhu, J. Su, F.-S. Zhang, Nucl. Phys. A **964**, 93 (2017)
44. L. Zhu, J. Su, W.-J. Xie, F.-S. Zhang, Phys. Lett. B **767**, 437 (2017)
45. C. Li, F. Zhang, J. Li et al., Phys. Rev. C **93**, 014618 (2016)
46. C. Li, P. Wen, J. Li et al., Phys. Lett. B **776**, 278 (2018)
47. C. Li, X. Xu, J. Li et al., Phys. Rev. C **99**, 024602 (2019)
48. F.-S. Zhang, C. Li, L. Zhu, P. Wen, Front. Phys. **13**, 132113 (2018)
49. V. Zagrebaev, W. Greiner, J. Phys. G Nucl. Part. Phys. **31**, 825 (2005)
50. V.I. Zagrebaev, W. Greiner, Phys. Rev. Lett. **101**, 122701 (2008)
51. V. Zagrebaev, W. Greiner, Nucl. Phys. A **834**, 366c (2010)
52. A.V. Karpov, V.V. Saiko, Phys. Rev. C **96**, 024618 (2017)
53. K. Sekizawa, K. Yabana, Phys. Rev. C **88**, 014614 (2013)
54. K. Sekizawa, S. Heinz, Acta Phys. Pol. B Proc. Suppl. **10**, 225 (2017)
55. L. Corradi, A.M. Vinodkumar, A.M. Stefanini et al., Phys. Rev. C **66**, 024606 (2002)
56. L. Corradi, G. Pollarolo, S. Szilner, J. Phys. G **36**, 113101 (2009)
57. F. Galtarossa, L. Corradi, S. Szilner et al., Phys. Rev. C **97**, 054606 (2018)
58. W. Krolas, R. Broda, B. Fornal et al., Nucl. Phys. A **724**, 289 (2003)
59. W. Krolas et al., Nucl. Phys. A **832**, 170 (2010)
60. C. Golabek, S. Heinz, W. Mittig et al., Eur. Phys. J. A **43**, 251 (2010)
61. V.F. Comas, S. Heinz, S. Hofmann et al., Eur. Phys. J. A **49**, 112 (2013)
62. O. Beliuskina, S. Heinz, V. Zagrebaev et al., Eur. Phys. J. A **50**, 161 (2014)
63. H.M. Devaraja, S. Heinz, O. Beliuskina et al., Phys. Lett. B **748**, 199 (2015)
64. S. Heinz, H.M. Devaraja, O. Beliuskina et al., Eur. Phys. J. A **52**, 278 (2016)
65. H.M. Devaraja, S. Heinz, D. Ackermann et al., Eur. Phys. J. A **55**, 25 (2019)
66. H.M. Devaraja, S. Heinz, D. Ackermann et al., Eur. Phys. J. A **56**, 224 (2020)
67. J.S. Barrett et al., Phys. Rev. C **91**, 064615 (2015)
68. V.V. Desai et al., Phys. Rev. C **99**, 044604 (2019)
69. Y.X. Watanabe, Y.H. Kim, S.C. Jeong et al., Phys. Rev. Lett. **115**, 172503 (2015)
70. Y. Hirayama, Y.X. Watanabe, N. Imai et al., Nucl. Instrum. Methods B **353**, 4 (2015)
71. J.V. Kratz, W. Loveland, K.J. Moody, Nucl. Phys. A **944**, 117 (2015)
72. R. Smolanczuk, A. Sobiczewski, Proceedings of the XV Nuclear Physics Divisional Conference on Low Energy Nuclear Dynamics, ed. by Yu.T. Oganessian et al. (World Scientific, Singapore, 1995), p. 313
73. M. Bender, K. Rutz, P.-G. Reinhard et al., Phys. Rev. C **60**, 034304 (1999)
74. M. Bender, Phys. Rev. C **61**, 031302 (2000)
75. S. Cwiok, W. Nazarewicz, P.H. Heenen, Phys. Rev. Lett. **83**, 1108 (1999)
76. S. Cwiok, P.-H. Heenen, W. Nazarewicz, Nature **433**, 705 (2005)
77. W.U. Schröder, J.R. Birkelund, J.R. Huizenga, Phys. Rep. **45**(5), 301 (1978)
78. V.V. Volkov, Phys. Rep. **44**, 93 (1978)
79. R. Bass, *Nuclear Reactions with Heavy Ions* (Springer, Berlin, 1980), p. 203
80. W. Nörenberg, in *Heavy Ion Collisions*, vol. 2, ed. by R. Bock (North-Holland, Amsterdam, 1980), p. 1
81. W.U. Schröder, J.R. Huizenga, in *Treatise on Heavy-Ion Science*, vol. 8, ed. by D.A. Bromley (Plenum Press, New York, 1989), p. 115
82. J. Wilczynski, Phys. Lett. B **47**, 484 (1973)
83. G.G. Adamian, N.V. Antonenko, W. Scheid, V.V. Volkov, Nucl. Phys. A **627**, 361 (1997)
84. V. Comas, S. Heinz, S. Hofmann et al., Eur. Phys. J. A **48**, 180 (2012)
85. D.J. Hinde et al., EPJ Web Conf. **131**, 04004 (2016)
86. M.G. Itkis, I.M. Itkis, G.N. Knyazheva, E.M. Kozulin, J. Phys. Conf. Ser. **863**, 012043 (2017)
87. M. Wilpert, B. Gebauer, Th. Wilpert et al., Phys. Rev. C **51**, 680 (1995)
88. S. Heinz, O. Beliuskina, V. Comas et al., Eur. Phys. J. A **51**, 140 (2015)
89. W. Bohne, P. Fröbrich, K. Grabisch et al., Z. Phys. A **313**, 19 (1983)
90. G. Guarino, A. Gobbi, K.D. Hildenbrand et al., Nucl. Phys. A **424**, 157 (1984)
91. P. Gippner, K.D. Schilling, W. Seidel et al., Z. Phys. A **325**, 335 (1986)
92. H. Freiesleben, K.D. Hildenbrand, F. Pühlhofer et al., Z. Phys. A **292**, 171 (1979)
93. A.G. Artukh, V.V. Avdeichikov, G.F. Gridnev et al., Phys. Lett. B **31**, 129 (1970)
94. M. Rejmund, B. Lecornu, A. Navin, C. Schmitt et al., Nucl. Inst. Methods Phys. Res. A **646**, 184 (2011)
95. E. Fioretto, F. Galtarossa, L. Corradi, H.M. Jia et al., Nucl. Inst. Methods Phys. Res. A **899**, 73 (2018)
96. A. Badala, M. La Cognata, R. Nania, M. Osipenko et al., La Rivista del Nuovo Cimento **45**, 189 (2022)
97. A. Di Nitto, J. Khuyagbaatar, D. Ackermann et al., Phys. Lett. B **784**, 199 (2018)
98. P. Schury, M. Wada, Y. Ito et al., Nucl. Instrum. Methods B **335**, 39 (2014)
99. Y. Hirayama, Y.X. Watanabe, N. Imai et al., Nucl. Instrum. Methods B **376**, 52 (2016)
100. T. Dickel, A. Kankainen, A. Spataru et al., J. Phys. Conf. Ser. **1668**, 012012 (2020). https://doi.org/10.1088/1742-6596/1668/1/012012
101. W.R. Plaß, T. Dickel, S. Purushothaman et al., Nucl. Instrum. Methods B **317**, 457 (2013)
102. C. Jesch, T. Dickel, W.R. Plaß et al., Nucl. Instrum. Methods A **777**, 172 (2015)
103. T. Dickel et al., Reaction studies with the FRS Ion Catcher: a novel approach and universal method for the production, identification of and experiments with unstable isotopes produced in multinucleon transfer reactions. Proposal to the G-PAC 2018/2019, proposal number S475 379
104. V.V. Saiko, A.V. Karpov, Acta Phys. Pol. B **50**, 495 (2019)
105. L. Zhu, J. Su, W.J. Xie, F.S. Zhang, Phys. Rev. C **94**, 054606 (2016)
106. Peng-Hui. Chen, Fei Niu, Xu. Xin-Xing, Zu-Xing. Yang et al., Phys. Rev. C **105**, 034610 (2022)
107. E.M. Kozulin, G.N. Knyazheva, K.V. Novikov et al., Phys. Rev. C **94**, 054613 (2016)
108. S. Heinz et al., Study of the dinuclear system $^{A}$Rb + $^{209}$Bi ($Z_1 + Z_2$ = 120). Proposal to the ISOLDE committee, CERNINTC-2012-043, INTC-P-344 (2012)
109. H.B. Yang, Z.Y. Zhang, J.G. Wang et al., Eur. Phys. J. A **51**, 88 (2015)
110. O.N. Malyshev, A.V. Belozerov, M.L. Chelnokov et al., Eur. Phys. J. A **8**, 295 (2000)

111. A.P. Leppänen, J. Uusitalo, M. Leino et al., Phys. Rev. C **75**, 054307 (2007)
112. A.N. Andreyev, D.D. Bogdanov, V.I. Chepigin et al., Z. Phys. A **338**, 363 (1991)
113. F.P. Heßberger, H. Gäggeler, P. Armbruster et al., Z. Phys. A **333**, 111 (1989)
114. A.V. Yeremin, D.D. Bogdanov, V.I. Chepigin, Nucl. Instrum. Methods A **350**, 608 (1994)
115. Z. Kalaninova, S. Antalic, F.P. Heßberger et al., Phys. Rev. C **92**, 014321 (2015)
116. J. Kurcewicz, F. Farinon, H. Geissel et al., Phys. Lett. B **717**, 371 (2012)
117. J. Taïeb, K.-H. Schmidt, L. Tassan-Got et al., Nucl. Phys. A **724**, 413 (2003)
118. T. Kurtukian-Nieto, J. Benlliure, K.-H. Schmidt et al., Phys. Rev. C **89**, 024616 (2014)
119. Myeong-Hwan. Mun, G.G. Adamian, N.V. Antonenko et al., Phys. Rev. C **89**, 034622 (2014)
120. F. Niu, P.-H. Chen, Y.-F. Guo, G.-W. Ma, Z.-Q. Feng, Phys. Rev. C **97**, 034609 (2018)
121. Long Zhu, Su. Cheng Li, Chen-Chen Guo. Jun, Wei Hua, Phys. Lett. B **791**, 20 (2019)